Wideband Beamforming with Frequency-Spatial Coupling in Near-Field Holographic ISAC

Tong Wei, Kumar Vijay Mishra, Linlong Wu, Bhavani Shankar M. R.
Interdisciplinary Centre for Security, Reliability and Trust (SnT), University of Luxembourg
email: {tong.wei@, kumar.mishra@ext., linlong.wu@, bhavani.shankar@}uni.lu

***Abstract*—This paper investigates the design of near-field wideband beamformers for holographic integrated sensing and communication (ISAC) to mitigate frequency-spatial-dependent beam split and near-field propagation effect with multiple moving targets. Specifically, we propose an efficient beamforming design strategy that leverages the properties of wideband signals and the frequency-spatial coupling of the near-field channel model in holographic ISAC systems which lead to high-dimension problem. The proposed scheme ensures high spatial resolution and robust performance in sensing tasks. We efficiently solve the resulting extremely large-scale nonconvex problem using the alternating direction method of multipliers (ADMM). Numerical experiments demonstrate that the proposed algorithm achieve favorable convergence performance, and the wideband near-field holographic ISAC can align beams toward multiple targets across different subcarriers.**

***Index Terms*—Alternating direction method of multipliers, near-filed holographic integrated sensing and communication.**

I. Introduction

Integrated sensing and communication (ISAC) systems have attracted significant research attention due to their ability to simultaneously provide communication and sensing functionalities through a unified platform [1–5]. Leveraging the radar sensing capabilities on wireless communications, ISAC systems can effectively utilize shared hardware resources, reduce deployment costs, and enhance spectrum efficiency [6]. This integrated framework is particularly advantageous for emerging wireless applications such as autonomous vehicles, intelligent transportation systems, and smart cities, where precise environmental perception and reliable signal transmission are essential [7].

Reconfigurable holographic surfaces (RHS), typically implemented using densely packed metasurface antenna arrays with sub-wavelength spacing, enable advanced electromagnetic wave manipulation to create programmable radio environments [8]. Different from another kind of metasurface, i.e., reconfigurable intelligent surfaces, RHS can quickly control the transmit beam toward to the desired directions with the low-cost and higher energy efficiency via tuning the amplitude of each RHS element [9, 10]. Exploring these advantages, RHS is utilized in communication system to significantly enhance spectral efficiency and spatial resolution [11]. By extending holographic technologies to ISAC, it can significantly amplify sensing accuracy and communication throughput due to its ability to precisely manipulate electromagnetic waves across a continuous aperture [12]. This increased flexibility facilitates advanced beamforming techniques, enabling holographic ISAC systems to better manage complex and dynamic propagation environments [13].

Recently, near-field beamforming techniques become critical when ISAC systems operate in short-range scenarios, where the classical far-field planar wave assumption no longer holds [14, 15]. Specifically, in the near-field region, wave propagation exhibits spherical wavefront characteristics, making traditional beamforming approaches ineffective. Thus, near-field ISAC must therefore account for the complex propagation behaviors and frequency-dependent spatial responses inherent to wideband signals [16]. After that, near-field holographic ISAC has garnered attention for its potential to achieve the improved downlink performance [17]. Most of the above-mentioned works assumed that the near-field channel achieves the flat pathloss over all the antennas which is not quiet matched with practical channel. Meanwhile, due to the utilizing of extremely large-scale antenna array in near-field applications, the resulting problem generally involves an extremely high dimension problem. These challenges necessitate efficient beamforming strategies that can dynamically adapt to the near-field characteristics of the holographic ISAC channel.

To address these issues, this paper proposes an efficient near-field wideband beamforming technique specifically designed for holographic ISAC systems. We leverage the unique properties of wideband signals and develop a frequency-spatial varying channel model tailored for near-field holographic propagation scenarios under the exact near-field channel model. To solve the resulting large-scale, highly nonconvex optimization problems, we apply the alternating direction method of multipliers (ADMM), demonstrating effective computational efficiency and convergence. Numerical experiments validate the effectiveness of our method, showing superior performance in aligning beams across multiple frequency subcarriers towards moving objectives, thus advancing its practical applicability.

II. Signal Model and Problem Formulation

Consider a wideband MIMO OFDM-ISAC system employing the extremely large-scale antenna array. The transmitter (Tx) and receiver (Rx) are equipped with a N_t-antenna RHS fed by N_{RF} radio-frequency (RF) chains, and N_r-antenna full-digital array. Both Tx and Rx are composed by uniform linear array (ULA) which can be either co-located or deployed separately. We denote $\mathbb{I}_{n_t} = (x_{n_t}, y_{n_t}), n_t \in \{1, \cdots, N_t\}$ and $\mathbb{I}_{n_r} = (x_{n_r}, y_{n_r}), n_r \in \{1, \cdots, N_r\}$ by the position of

n_t-th Tx antenna and n_r-th Rx antenna, respectively, in a two-dimensional (2-D) Cartesian plane. Assume that the holographic ISAC system senses the near-field coverage area comprised Q targets, a term which refers to the objects of interest to radar, communication users [1], and scatterers; the q-th target located at $\mathbb{I}_q$ and having a velocity $\boldsymbol{v}^{(q)}, q = 1, \cdots, Q$.

The OFDM signaling consists of K subcarriers and M OFDM symbols, each with a total duration of $T_{\rm sym} = T_{\rm cp} + T_{\rm es}$, where $T_{\rm cp}$ and $T_{\rm es}$ represent the cyclic prefix duration and elementary symbol duration, respectively. The subcarrier spacing is given by $\triangle f = \frac{1}{T_{\rm es}}$. Furthermore, the frame length of the coherent processing interval (CPI) is defined as $T_{\rm cpi} = MT_{\rm sym}$ [19, 20]. Let the signal vector transmitted on k-th subcarrier and m-th OFDM symbol over N_t antennas be denoted by $\mathbf{x}_{k,m} \in \mathbb{C}^{N_t \times 1}$.

A. Wideband Holographic Transmission Model

Following the holographic principle [10, 21], the transmit signal at k-th subcarrier and m-th OFDM symbol over N_t antennas is

$$\mathbf{x}_{k,m} = \mathbf{\Psi}\mathbf{V}_k\mathbf{F}_k\mathbf{s}_{k,m} \in \mathbb{C}^{N_t \times 1} \tag{1}$$

where $\mathbf{F}_k \in \mathbb{C}^{N_{RF} \times U}$ denotes full-digital beamformer, $\mathbf{s}_{k,m} \in \mathbb{C}^{U \times 1}$ denotes the data symbols for the communication users [22–24], $U \leq Q$ denotes the total number of communication users, $\mathbf{V}_k \in \mathbb{C}^{N_t \times N_{RF}}$ denotes the propagation delay matrix of RHS at the k-th subcarrier with $\mathbf{V}_k(n_t, n_{RF}) = e^{-j2\pi\gamma\frac{d_{n_{RF},n_t}}{\lambda_k}}$, $n_t = 1, \cdots, N_t$ and $n_{RF} = 1, \cdots, N_{RF}$, γ denotes the radiation profile of the RHS material, d_{n_{RF},n_t} denotes the distance between n_{RF}-th RF chain and n_t-th RHS element, and the diagonal matrix $\mathbf{\Psi} \in \mathbb{R}^{N_t \times N_t}$ denotes the holographic beamformer. Applying N_t K-point inverse fast Fourier transform (IFFT) to the signal $\mathbf{x}_{k,m}$, and following an upconversion over the block of M symbols in $t \in [0, MT_{sym}]$, the transmit signal of RHS element in time domain takes the form [20, 22]

$$\widetilde{\mathbf{x}}(t) = \Re\left\{\sum_{m=1}^{M}\sum_{k=1}^{K}\mathbf{x}_{k,m}e^{j2\pi f_k t}\mathrm{rect}\left(\frac{t - mT_{\rm sym}}{T_{\rm sym}}\right)\right\} \tag{2}$$

where the rectangular pulse function $\mathrm{rect}(t)$ takes the value 1 for $t \in [0, 1]$ and 0 otherwise, f_c is the carrier frequency and $f_k = f_c + k\triangle f$ is the k-th subcarrier frequency.

B. Near-field Sensing Model

The received signal at n_r-th receive antenna after propagation delay is

$$y_{n_r}(t) = \sum_{q=1}^{Q}\alpha_q g^q_{n_r}(t)\sum_{n_t=1}^{N_t} g^q_{n_t}(t)\widetilde{x}_{n_t}(t - \tau^q_{n_t n_r})e^{j2\pi f^{q,k}_{n_t n_r} t} + n_{n_r}(t), \tag{3}$$

where α_q denotes the RCS of q-th target and $n_{n_r}(t)$ is the front end additive Gaussian white noise (AWGN) of the n_r-th Rx element. The Doppler shift, $f^{q,k}_{n_t n_r}$, for the q-th target on the k-th subcarrier with the n_t-th Tx and n_r-th Rx antenna pair is given [25]

$$f^{q,k}_{n_t n_r} = \frac{f_k}{c}\left(\frac{\langle \boldsymbol{v}^{(q)}, \mathbb{I}_q - \mathbb{I}_{n_t}\rangle}{\|\mathbb{I}_q - \mathbb{I}_{n_t}\|} + \frac{\langle \boldsymbol{v}^{(q)}, \mathbb{I}_q - \mathbb{I}_{n_r}\rangle}{\|\mathbb{I}_q - \mathbb{I}_{n_r}\|}\right), \tag{4}$$

where $\boldsymbol{v}^{(q)} = [v_x^{(q)}, v_y^{(q)}]$ denotes the directional velocity of q-th target in which $v_x^{(q)}$ and $v_y^{(q)}$ are the velocity along with x and y-axis, respectively [26]. Meanwhile, the time delay in (3) takes the form

$$\tau^q_{n_t n_r} = \frac{\|\mathbb{I}_q - \mathbb{I}_{n_t}\| + \|\mathbb{I}_q - \mathbb{I}_{n_r}\|}{c}. \tag{5}$$

We consider frequency-dependent path loss in (3) which can be modeled as $g^q_{*,k} = \sqrt{z_*}\frac{\lambda_k}{4\pi\|\mathbb{I}_q - \mathbb{I}_*\|}$ [27], where $* \in \{n_r, n_t\}$, z_* denotes radiation profile of the material of corresponding element, and $z_* = 1$ for the full-digital array and $0 < z_* < 1$ for RHS [28].

Removing CP and the carrier frequency in I/Q demodulation and implementing the Fourier transform within m-th time interval i.e., OFDM symbol duration, the received signal on the k-th subcarrier of the m-th OFDM symbol is given by

$$y_{n_r}[m, k] = \int_{mT_{\rm sym}+T_{\rm cp}}^{(m+1)T_{\rm sym}} y_{n_r}(t)e^{-2\pi f_c t}e^{-2\pi k\triangle f t}dt. \tag{6}$$

Substituting (3) into (6) and stacking the received signal of all the Rx elements, we can rewrite (6) as

$$\mathbf{y}_{k,m} = \sum_{q=1}^{Q}\alpha_q\mathbf{a}_{\rm R}(k, m, q)\mathbf{a}^T_{\rm T}(k, m, q)\mathbf{x}_{k,m} + \mathbf{n}_{k,m}, \tag{7}$$

$$\mathbf{a}_{\rm T}(k, m, q) = [g^q_{1,k}e^{j2\pi\varphi_1(k,m,q)}, \cdots, g^q_{N_t,k}e^{j2\pi\varphi_{N_t}(k,m,q)}]^T,$$

$$\varphi_*(k, m, q) = \frac{f_k}{c}\left(\frac{\langle \boldsymbol{v}^{(q)}, \mathbb{I}_q - \mathbb{I}_*\rangle}{\|\mathbb{I}_q - \mathbb{I}_*\|}mT_{\rm sym} - \|\mathbb{I}_q - \mathbb{I}_*\|\right),$$

and $* \in \{n_t, n_r\}$, where $\mathbf{a}_{\rm T}$ denotes the wideband near-field Tx steering vector of Tx; the Rx steering vector is similarly defined. We then stack the received signal (7) from all M OFDM symbols into a single vector as

$$\mathbf{y}_k = \mathbf{A}_k\mathbf{x}_k + \mathbf{n}_k \in \mathbb{C}^{N_r M} \tag{8}$$

where $\mathbf{y}_k = [\mathbf{y}^T_{k,1}, \cdots, \mathbf{y}^T_{k,M}]^T$ denotes the receive signal of k-th subcarrier with the mean $\boldsymbol{\mu}_k = \mathbf{A}_k\mathbf{x}_k$ and the covariance $\mathbf{C}_k = \sigma_r^2\mathbf{I}_{N_r M}$ respectively, $\mathbf{A}_k = \mathrm{bdiag}[\mathbf{A}_{k,1}, \cdots, \mathbf{A}_{k,M}]$, $\mathbf{x}_k = [\mathbf{x}^T_{k,1}, \cdots, \mathbf{x}^T_{k,M}]^T$ and $\mathbf{n}_k = [\mathbf{n}^T_{k,1}, \cdots, \mathbf{n}^T_{k,M}]^T$.

C. Problem formulation

Let us first rewrite (8) as the real vector $\bar{\mathbf{y}}_k = [\Re(\mathbf{y}_k)^T; \Im(\mathbf{y}_k)^T]^T$, $\bar{\boldsymbol{\mu}}_k = [\Re(\boldsymbol{\mu}_k)^T, \Im(\boldsymbol{\mu}_k)^T]^T$, and $\bar{\mathbf{C}}_k = \frac{\sigma_r^2}{2}\mathbf{I}_{2N_r M}$. To evaluate the performance of beamformers, we can first write the likelihood function as [29]

$$p_k(\bar{\mathbf{y}}_k, \mathbf{x}_k) = \frac{1}{\sqrt{2\pi^{2N_r M}|\bar{\mathbf{C}}_k|}}e^{-(\bar{\mathbf{y}}_k - \bar{\boldsymbol{\mu}}_k)^T\bar{\mathbf{C}}_k^{-1}(\bar{\mathbf{y}}_k - \bar{\boldsymbol{\mu}}_k)/2}. \tag{9}$$

[1]Herein, we assumed that the communication users can also reflect the signal to Rx for estimating and tracking the key motion parameters, see [18].

According to (9), we can write the log-likelihood function and omit the constant terms as

$$\ln p_k(\bar{\mathbf{y}}_k, \mathbf{x}_k) = -\frac{1}{2}(\ln|\bar{\mathbf{C}}_k| + (\bar{\mathbf{y}}_k - \bar{\boldsymbol{\mu}}_k)^T \bar{\mathbf{C}}_k^{-1}(\bar{\mathbf{y}}_k - \bar{\boldsymbol{\mu}}_k)).$$

For the near-field transmit beamformer design, we can assume the channel matrix $\mathbf{A}_k$ is obtained and then solve the following problem

$$\underset{\mathbf{x}_k, k=1\cdots,K}{\text{maximize}} \quad \sum_{k=1}^{K} \ln p_k(\mathbf{y}_k, \boldsymbol{\theta}^{(t)}) \tag{10a}$$

$$\text{subject to} \quad \|\mathbf{x}_k\|_2^2 = \mathcal{P}_k, \forall k, \tag{10b}$$

where the constraint restrict the transmit power in the certain level. Herein, an equality constraint is imposed on the total power budget in (10), as practical radar systems typically operate at their maximum available transmit power [6, 30]. Similarly, we rewrite the non-negative log-likelihood function to MSE as [31]

$$\underset{\mathbf{x}_k, k=1\cdots,K}{\text{minimize}} \quad \sum_{k=1}^{K} \|\mathbf{y}_k - \mathbf{A}_k\mathbf{x}_k\|_2^2 \tag{11a}$$

$$\text{subject to} \quad \|\mathbf{x}_k\|_2^2 = \mathcal{P}_k, \forall k. \tag{11b}$$

Lemma 1. *The strong duality holds for nonconvex problem* (10) *under the mild condition* $\mathcal{P}_k > 0$.

Proof. See [32]. □

Based on Lemma 1, the global optimal solution of nonconvex problem (10) can be achieved using the primal dual method or the SDR method [33, 34]. However, solving the dual problem involves a set of nonlinear equation which lead to a higher computational complexity.

III. ADMM Solver

To tackle the challenging nonconvex problem (11), we utilize ADMM to solve the problem with a lower complexity. Because of the disjoint variables and the objective function, for k-th subcarrier, we can first reformulate problem (11) equivalently

$$\underset{\mathbf{x}_k, \mathbf{z}_k}{\text{minimize}} \quad \|\mathbf{y}_k - \mathbf{A}_k\mathbf{x}_k\|_2^2 \tag{12a}$$

$$\text{subject to} \quad \mathbf{z}_k^H\mathbf{z}_k = \mathcal{P}_k, \tag{12b}$$

$$\mathbf{z}_k - \mathbf{x}_k = \mathbf{0}. \tag{12c}$$

Lemma 2. *The strong duality holds for nonconvex problem* (12) *under the mild condition* $\mathcal{P}_k > 0$.

Proof. We omit the proof due to the limited space. □

We can use Lemma 2 to analyze the convergence and global optimality which are beyond the scope of this paper and thus omit herein. Note that the problem in (12) is separate in terms of the subcarrier index k. We can solve the problems in parallel for all subcarriers. Then, the augmented Lagrangian of problem (12) is given by

$$\begin{aligned}\mathcal{L}(\mathbf{x}_k, \mathbf{z}_k, \mathbf{u}_k) =& \mathbf{x}_k^H\mathbf{A}_k^H\mathbf{A}_k\mathbf{x}_k - 2\Re(\mathbf{y}_k^H\mathbf{A}_k\mathbf{x}_k) + \mathbf{y}_k^H\mathbf{y}_k \\ &+ \Re(\mathbf{u}_k^H(\mathbf{z}_k - \mathbf{x}_k)) + \frac{\rho_k}{2}\|\mathbf{z}_k - \mathbf{x}_k\|_2^2. \end{aligned} \tag{13}$$

Based on the equality,

$$\Re(\mathbf{u}_k^H(\mathbf{z}_k - \mathbf{x}_k)) + \frac{\rho_k}{2}\|\mathbf{z}_k - \mathbf{x}_k\|_2^2 \tag{14}$$

$$= \frac{\rho_k}{2}\|\mathbf{z}_k - \mathbf{x}_k + \frac{1}{\rho_k}\mathbf{u}_k\|_2^2 - \frac{1}{2\rho_k}\|\mathbf{u}_k\|_2^2$$

$$= \frac{\rho}{2}\|\mathbf{z}_k - \mathbf{x}_k + \mathbf{v}_k\|_2^2 - \frac{\rho_k}{2}\|\mathbf{v}_k\|_2^2, \tag{15}$$

where $\mathbf{v}_k = \frac{1}{\rho_k}\mathbf{u}_k$, we can write the augmented Lagrangian (13) as

$$\begin{aligned}\mathcal{L}(\mathbf{x}_k, \mathbf{z}_k, \mathbf{v}_k) =& \mathbf{x}_k^H\mathbf{A}_k^H\mathbf{A}_k\mathbf{x}_k - 2\Re(\mathbf{y}_k^H\mathbf{A}_k\mathbf{x}_k) + \mathbf{y}_k^H\mathbf{y}_k \\ &+ \frac{\rho_k}{2}\|\mathbf{z}_k - \mathbf{x}_k + \mathbf{v}_k\|_2^2 - \frac{\rho_k}{2}\|\mathbf{v}_k\|_2^2. \end{aligned} \tag{16}$$

A. ADMM Solution

Then, the ADMM update for jointly solving the primal-dual problem (12) as

$$\begin{aligned}\mathbf{x}_k^{(t+1)} = \underset{\mathbf{x}_k}{\text{argmin}}\ & \mathbf{x}_k^H\mathbf{A}_k^H\mathbf{A}_k\mathbf{x}_k - 2\Re(\mathbf{y}_k^H\mathbf{A}_k\mathbf{x}_k) \\ &+ \frac{\rho_k}{2}\|\mathbf{z}_k^{(t)} - \mathbf{x}_k + \mathbf{v}_k^{(t)}\|_2^2; \end{aligned} \tag{17a}$$

$$\mathbf{z}_k^{(t+1)} = \underset{\mathbf{z}_k}{\text{argmin}}\ \frac{\rho_k}{2}\|\mathbf{z}_k - \mathbf{x}_k^{(t)} + \mathbf{v}_k^{(t)}\|_2^2,\ \text{s.t. } \mathbf{z}_k^H\mathbf{z}_k = \mathcal{P}_k; \tag{17b}$$

$$\mathbf{v}_k^{(t+1)} = \underset{\mathbf{v}_k}{\text{argmax}}\ \frac{\rho_k}{2}\|\mathbf{z}_k^{(t)} - \mathbf{x}_k^{(t)} + \mathbf{v}_k\|_2^2 - \frac{\rho_k}{2}\|\mathbf{v}_k\|_2^2. \tag{17c}$$

Then, the solutions for the subproblems in (17) are, respectively, given by

$$\mathbf{x}_k^{(t+1)} = (\mathbf{A}_k^H\mathbf{A}_k + \frac{\rho_k}{2}\mathbf{I})^{-1}(\mathbf{A}_k^H\mathbf{y}_k + \frac{\rho_k}{2}(\mathbf{z}_k^{(t)} + \mathbf{v}_k^{(t)})); \tag{18a}$$

$$\mathbf{z}_k^{(t+1)} = \frac{\mathcal{P}_k}{\|\mathbf{x}_k^{(t+1)} - \mathbf{v}_k^{(t)}\|_2}(\mathbf{x}_k^{(t+1)} - \mathbf{v}_k^{(t)}); \tag{18b}$$

$$\mathbf{v}_k^{(t+1)} = \mathbf{v}_k^{(t)} + \mathbf{z}_k^{(t+1)} - \mathbf{x}_k^{(t+1)}. \tag{18c}$$

It is seen that the updating of $\mathbf{x}_k$ in (18a) involves the inverse of the large-scale matrix which leads to the extremely high computational complexity. Toward this end, we can use the block sparse property of matrix $\mathbf{A}_k$ to simplify the calculation of the inverse matrix, i.e., $\mathbf{A}_k^{-1} = \text{bdiag}[\mathbf{A}_{k,1}^{-1}, \cdots, \mathbf{A}_{k,M}^{-1}]$. Note that for the problem (18b), it should chose the scalar as $\frac{\sqrt{\mathcal{P}_k}}{\|\mathbf{x}_k^{(t+1)} - \mathbf{v}_k^{(t)}\|_2}$ but not $-\frac{\sqrt{\mathcal{P}_k}}{\|\mathbf{x}_k^{(t+1)} - \mathbf{v}_k^{(t)}\|_2}$ due to the second-order optimal condition.

Once the optimal transmit beamformers over all aubcarriers are obtained by ADMM, the full-digital and holographic beamformers can be determined by the following optimization problem

$$\underset{\boldsymbol{\Psi}, \mathbf{f}_{k,m}}{\text{minimize}} \quad \sum_{k=1}^{K}\sum_{m=1}^{M} \|\mathbf{x}_{k,m} - \boldsymbol{\Psi}\mathbf{V}_k\mathbf{f}_{k,m}\|_2^2 \tag{19a}$$

$$\text{subject to} \quad 0 \le \psi_{n_t} \le 1, n_t = 1, \cdots, N_t, \tag{19b}$$

where $\mathbf{f}_{k,m} = \mathbf{F}_{k,m}\mathbf{s}_{k,m}$. We observed that in (19), the problems in terms of $\boldsymbol{\Psi}$ and $\mathbf{f}_{k,m}$, respectively, are convex. Then, it can be efficiently solved by the alternating optimization method.

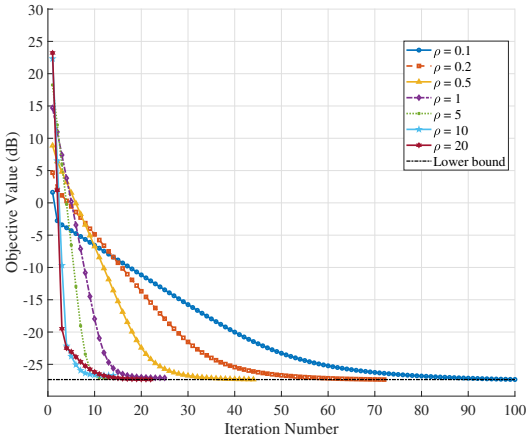

Figure 1. Convergence performance of ADMM algorithm.

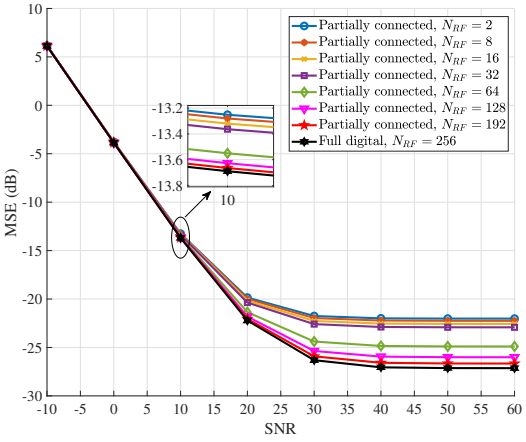

Figure 2. MSE versus SNR.

B. Complexity Analysis

In general, the interior-point method for SDP algorithm has worst-case complexity $\mathcal{O}(K(MN_t)^6)$ even tough it guarantees globally optimal solution [34]. Meanwhile, the complexity of proposed ADMM algorithm of each iteration is $\mathcal{O}(K(MN_t)^3)$ for calculating the matrix inversion in (18a). Thus, the total complexity of the proposed ADMM algorithm is $\mathcal{O}(TK(MN_t)^3)$, where T denotes the total number of iterations. However, due to the block diagonal spare structure of $\mathbf{A}_k$, the complexity of SDR can be reduced to $\mathcal{O}(KM(N_t)^{3.5})$. Meanwhile, the complexity of proposed ADMM algorithm can reach to $\mathcal{O}(TKM(N_t)^2)$ which is much less than SDR. It shows the efficiency of the proposed ADMM algorithm, especially in the case of a wideband near-field and extremely large-scale problem.

IV. Numerical Experiments

In the simulations, we consider a holographic system with $N_t = 256$ and $N_r = 128$ that is deployed along the x-axis and set the origin as the centroid. The inter-element spacings for Tx and Rx are set to $\lambda_c/4$ and $\lambda_c/2$ with $z_{n_t} = 0.8, \forall n_t$ and $z_{n_r} = 1, \forall n_r$. The number of RF chains is $N_{RF} = 16$. The central frequency of the wideband ISAC system is $f_c = 28$ GHz, and the frequency step of OFDM is set to $\triangle f = 20$ MHz. The total number of subcarriers and OFDM symbols are set to $K = 16$ and $M = 8$. Three objectives are located on $[48, 54]$, $[-36, 48]$, and $[0, 54]$, referred to radar target, communication user, and scatterer respectively with the velocities of $[10, 10]$, $[1, 1]$, and $[0, 0]$ m/s. The RCS in terms of all objectives are set to $|\alpha_1| = 1$, $|\alpha_2| = 1$, and $|\alpha_3| = 0.1$. The noise variances are $\sigma_r^2 = -80$dB and the Lagrangian parameters $\rho_1 = \cdots = \rho_K$. We terminate the ADMM algorithm when the error between two adjacent iterations less than 10^{-5} or reaches the maximal iteration number $t_{max} = 100$.

Fig. 1 illustrates the convergence of ADMM algorithm for solving the problem (12). It is seen that, as the increasing of iteration, the objective value of problem (12) is monotonically decreased and convergent within 100 iterations. Meanwhile, the increasing of Lagrangian parameter first fasts the convergence speed until $\rho_k = 10$ and then slows down the convergence property. This highlights the importance of Lagrangian parameter selection.

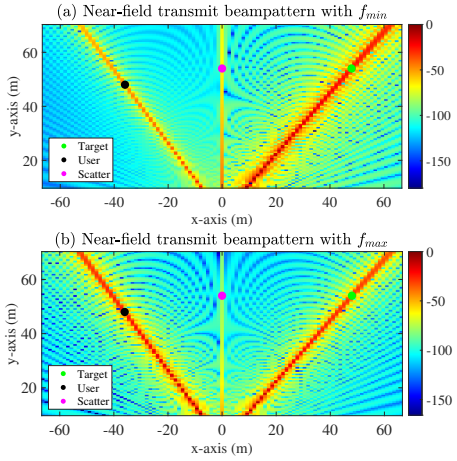

Figure 3. Comparison of transmit beampattern in different subcarriers.

Fig. 2 demonstrates the MSE versus the SNR under different number of RF chains. It is observed that with the increasing number of RF chain, the performance of partially connected structure approaches the fully connected structure in which each RF chain is connected with an RHS element. Meanwhile, in low SNR case, i.e., less than 10 dB, the proposed holographic can still achieve a preferable performance with a few RF chain, e.g., $N_{RF} = 2$.

Fig. 3 shows the transmit beampattern of Tx with RHS. Specifically, Fig. 3(a) and Fig. 3(b) illustrate the transmit beampattern on the lowest frequency band f_{min} and highest frequency band f_{max}, respectively. It is seen that the proposed wideband near-field beamforming scheme can align the beam toward to the directions of objectives in different subcarrier. This validates the effectiveness of our proposed method.

V. Summary

This paper has addressed the problem of near-field wideband beamforming in holographic ISAC systems. The proposed beamforming strategy leverages frequency-spatial channel characteristics to deliver high spatial resolution and robust sensing performance. The resulting nonconvex problem is solved efficiently by ADMM algorithm. Numerical results demonstrate that the proposed solution effectively aligns beams toward dynamically moving targets across various frequencies, highlighting significant improvements in practical applicability. Future research could further explore the near-field parameter estimation to further enhance the near-field beamformer design.

Acknowledgment

This work was supported by the Luxembourg National Research Fund (FNR) through the CORE Project S3 under grant C22/IS/17412681/S3.

References

[1] K. V. Mishra, M. B. Shankar, V. Koivunen, B. Ottersten, and S. A. Vorobyov, "Toward millimeter-wave joint radar communications: A signal processing perspective," *IEEE Signal Processing Magazine*, vol. 36, no. 5, pp. 100–114, 2019.

[2] Z. Wei, H. Qu, Y. Wang, X. Yuan, H. Wu, Y. Du, K. Han, N. Zhang, and Z. Feng, "Integrated sensing and communication signals toward 5G-A and 6G: A survey," *IEEE Internet of Things Journal*, vol. 10, no. 13, pp. 11 068–11 092, 2023.

[3] T. Wei, L. Wu, K. V. Mishra, and M. R. B. Shankar, "Multi-IRS-aided Doppler-tolerant wideband DFRC system," *IEEE Transactions on Communications*, vol. 71, no. 11, pp. 6561–6577, 2023.

[4] S. Nayemuzzaman, K. V. Mishra, J. Liu, and M. Saquib, "Co-designing statistical MIMO radar and in-band full-duplex multi-user MIMO communications–part III: Multi-target tracking," *arXiv preprint arXiv:2403.19120*, 2024.

[5] E. Vargas, K. V. Mishra, R. Jacome, B. M. Sadler, and H. Arguello, "Dual-blind deconvolution for overlaid radar-communications systems," *IEEE Journal on Selected Areas in Information Theory*, vol. 4, pp. 75–93, 2023.

[6] K. V. Mishra, M. Bhavani Shankar, B. Ottersten, and A. L. Swindlehurst, *Signal Processing for Joint Radar Communications*. Wiley-IEEE Press, 2024.

[7] A. Hassanien, M. G. Amin, E. Aboutanios, and B. Himed, "Dual-function radar communication systems: A solution to the spectrum congestion problem," *IEEE Signal Processing Magazine*, vol. 36, no. 5, pp. 115–126, 2019.

[8] R. Deng, B. Di, H. Zhang, D. Niyato, Z. Han, H. V. Poor, and L. Song, "Reconfigurable holographic surfaces for future wireless communications," *IEEE Wireless Communications*, vol. 28, no. 6, pp. 126–131, 2021.

[9] S. Zeng, H. Zhang, B. Di, H. Qin, X. Su, and L. Song, "Reconfigurable refractive surfaces: An energy-efficient way to holographic MIMO," *IEEE Communications Letters*, pp. 1–1, 2022.

[10] T. Wei, L. Wu, K. V. Mishra, and B. Shankar M. R., "RIS-aided wideband holographic DFRC," *IEEE Transactions on Aerospace and Electronic Systems*, vol. 60, no. 4, pp. 4241–4256, 2024.

[11] R. Deng, B. Di, H. Zhang, Y. Tan, and L. Song, "Reconfigurable holographic surface-enabled multi-user wireless communications: Amplitude-controlled holographic beamforming," *IEEE Transactions on Wireless Communications*, vol. 21, no. 8, pp. 6003–6017, 2022.

[12] H. Zhang, H. Zhang, B. Di, M. D. Renzo, Z. Han, H. V. Poor, and L. Song, "Holographic integrated sensing and communication," *IEEE Journal on Selected Areas in Communications*, vol. 40, no. 7, pp. 2114–2130, 2022.

[13] H. Zhang, H. Zhang, B. Di, and L. Song, "Holographic integrated sensing and communications: Principles, technology, and implementation," *IEEE Communications Magazine*, vol. 61, no. 5, pp. 83–89, 2023.

[14] A. M. Elbir, Ö. T. Demir, K. V. Mishra, S. Chatzinotas, and M. Haardt, "Near-field signal processing: Unleashing the power of proximity," *IEEE Signal Processing Magazine*, 2025, in press.

[15] Z. Wang, X. Mu, and Y. Liu, "Near-field integrated sensing and communications," *IEEE Communications Letters*, vol. 27, no. 8, pp. 2048–2052, 2023.

[16] X. Wang, W. Zhai, X. Wang, M. G. Amin, and K. Cai, "Wideband near-field integrated sensing and communication with sparse transceiver design," *IEEE Journal of Selected Topics in Signal Processing*, vol. 18, no. 4, pp. 662–677, 2024.

[17] B. Zhao, C. Ouyang, X. Zhang, and Y. Liu, "Performance analysis of holographic MIMO based integrated sensing and communications," *IEEE Transactions on Communications*, 2025, in press.

[18] Z. Hu, Q. Ye, Y. Huang, S. Hu, and G. Yang, "Joint range-velocity-azimuth estimation for OFDM-based integrated sensing and communication," *IEEE Transactions on Wireless Communications*, vol. 23, no. 10, pp. 12 933–12 948, 2024.

[19] Y. Liu, G. Liao, Y. Chen, J. Xu, and Y. Yin, "Super-resolution range and velocity estimations with OFDM integrated radar and communications waveform," *IEEE Transactions on Vehicular Technology*, vol. 69, no. 10, pp. 11 659–11 672, 2020.

[20] M. F. Keskin, V. Koivunen, and H. Wymeersch, "Limited feedforward waveform design for OFDM dual-functional radar-communications," *IEEE Transactions on Signal Processing*, vol. 69, pp. 2955–2970, 2021.

[21] B. Di, "Reconfigurable holographic metasurface aided wideband OFDM communications against beam squint," *IEEE Transactions on Vehicular Technology*, vol. 70, no. 5, pp. 5099–5103, 2021.

[22] L. Zheng and X. Wang, "Super-resolution delay-doppler estimation for OFDM passive radar," *IEEE Transactions on Signal Processing*, vol. 65, no. 9, pp. 2197–2210, 2017.

[23] Y. Li, X. Wang, and Z. Ding, "Multi-target position and velocity estimation using OFDM communication signals," *IEEE Transactions on Communications*, vol. 68, no. 2, pp. 1160–1174, 2020.

[24] Z. Xu and A. Petropulu, "A bandwidth efficient dual-function radar communication system based on a MIMO radar using OFDM waveforms," *IEEE Transactions on Signal Processing*, vol. 71, pp. 401–416, 2023.

[25] S. Sun, Y. Hu, K. V. Mishra, and A. P. Petropulu, "Widely separated MIMO radar using matrix completion," *IEEE Transactions on Radar Systems*, vol. 2, pp. 180–196, 2024.

[26] S. Sun, K. V. Mishra, and A. P. Petropulu, "Target estimation by exploiting low rank structure in widely separated MIMO radar," in *IEEE Radar Conference*, 2019, pp. 1–6.

[27] K. Dovelos, M. Matthaiou, H. Q. Ngo, and B. Bellalta, "Channel estimation and hybrid combining for wideband terahertz massive MIMO systems," *IEEE Journal on Selected Areas in Communications*, vol. 39, no. 6, pp. 1604–1620, 2021.

[28] J. Xu, L. You, G. C. Alexandropoulos, X. Yi, W. Wang, and X. Gao, "Near-field wideband extremely large-scale MIMO transmissions with holographic metasurface-based antenna arrays," *IEEE Transactions on Wireless Communications*, pp. 1–1, 2024.

[29] P. Stoica and R. Moses, *Spectral analysis of signals*. Pearson Prentice Hall, 2005.

[30] J. Li, L. Xu, P. Stoica, K. W. Forsythe, and D. W. Bliss, "Range compression and waveform optimization for MIMO radar: A Cramér–Rao bound based study," *IEEE Transactions on Signal Processing*, vol. 56, no. 1, pp. 218–232, 2008.

[31] H. Hua, J. Xu, and Y. C. Eldar, "Near-field 3D localization via MIMO radar: Cramér-Rao bound analysis and estimator design," *IEEE Transactions on Signal Processing*, vol. 72, pp. 3879–3895, 2024.

[32] T. Pham Dinh and A. Le Thi Hoai, "Lagrangian stability and global optimality in nonconvex quadratic minimization over Euclidean balls and spheres." *Journal of Convex Analysis*, vol. 2, no. 1-2, pp. 263–276, 1995.

[33] Y. Huang and D. P. Palomar, "Rank-constrained separable semidefinite programming with applications to optimal beamforming," *IEEE Transactions on Signal Processing*, vol. 58, no. 2, pp. 664–678, 2010.

[34] Z.-Q. Luo, W.-K. Ma, A. M.-C. So, Y. Ye, and S. Zhang, "Semidefinite relaxation of quadratic optimization problems," *IEEE Signal Processing Magazine*, vol. 27, no. 3, pp. 20–34, 2010.